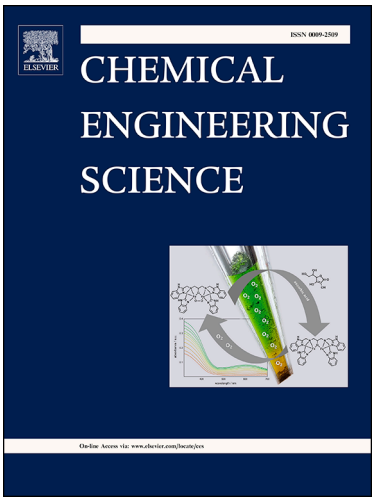

Synchronous screening-and-optimization of nano-engineered blood pressure-drop using rapid robust non-linear Taguchi profiling

George J Besseris

PII: S0009-2509(19)30251-9
DOI: https://doi.org/10.1016/j.ces.2019.03.035
Reference: CES 14858

To appear in: *Chemical Engineering Science*

Received Date: 16 October 2018
Revised Date: 10 March 2019
Accepted Date: 15 March 2019

Please cite this article as: G.J. Besseris, Synchronous screening-and-optimization of nano-engineered blood pressure-drop using rapid robust non-linear Taguchi profiling, *Chemical Engineering Science* (2019), doi: https://doi.org/10.1016/j.ces.2019.03.035

Synchronous screening-and-optimization of nano-engineered blood pressure-drop using rapid robust non-linear Taguchi profiling.

George J Besseris*

Mechanical Engineering Department,

University of West Attica

Aigaleo, Attica, Greece

*Email address: besseris@uwa.gr

And

Advanced Industrial and Manufacturing Systems

Kingston University, London, UK.

Abstract

Atherosclerosis induces abnormal blood-flow patterns in coronary arteries mainly because of the irregular accumulation of fibrofatty plaque on the artery walls. Morphological alterations of the wall-surface attributes downgrade vascular elasticity, which compromises the normal blood-pressure gradient behavior by sporadically interfering with the effective-flow cross-section adjustment. An iron-oxide booster has been recently studied as a potential nano-particle treatment to regulate an elevated blood-pressure condition. Taguchi-type multi-factorial experimentation rapidly generates small and dense datasets in order to expedite arterial flow screening/optimization predictions. The optimal blood pressure-drop performance is investigated against four vital controlling factors. We show that tracking down inherently complex blood-flow phenomena often entails the elucidation of non-linear and messy data structures. Translating such data demands robust and agile techniques to decipher governing relationships while guarding against spurious effects from uncertainty asymmetry. We also show that by using distribution-free profiling, we may synchronously accomplish the screening and optimization tasks more accurately in comparison to other competing techniques. Illustrating our technique on a chemical engineering paradigm, we found that out of the four investigated factors only the blood behavior index to be strongly influential. A blood behavior index setting of 0.5, which is below the normal physiological limit, minimizes the blood pressure drop at an optimal value of 385 Pa/m. The proposed methodology demonstrates how the required sampling size may be further reduced, thus making the study even more economically

and practically efficient. This was shown to be achieved without relinquishing important information about the dominant phenomena, hence rendering our solution to be also lean and agile.

Keywords: Atherosclerotic coronary artery, nano-bioengineering, screening/optimization engineering, robust blood pressure-drop profiling, non-linear non-normal data, data messiness.

1. Introduction

Blood is a non-Newtonian bio-fluid that nourishes a mammalian organism and partakes in sustaining its normal physiological condition. Modeling the complex multiphase flow of blood in normal and pathophysiological cases has been the subject of several chemical engineering studies [1-4]. The practical implications of attempting to delineate the complexity of the blood flow behavior in several situations, with great engineering interest, such as at interfaces[5], in suspension concentrations[6] and for modified vascularity propensities[7], pose continuous challenges. Among the most intriguing blood flow phenomena that currently attract the attention of modern biomedical engineering and chemical bioengineering areas deal with novel applications that promote the efficient regulation of blood pressure abnormalities. Primarily, the emphasis is placed on the treatment and prevention of the atherosclerosis disease[8]. Advances in popular nanomedicine aim to assist all three relevant phases: diagnosis, treatment and monitoring [9-12]. Managing to recommend maintenance tactics for lowering high blood pressure levels is susceptible to plenty of factors. It requires deep knowledge about how atherosclerosis impairs the function of a coronary artery network. Nanoparticle-based diagnosis and drug delivery may be ameliorated by encompassing state of the art chemical engineering know-how [13-15]. For example, nanoparticles could be applied as drug carriers to mediate the underlying hemodynamics in a stenotic vascular channel [16-20]. A promising screening study in atherosclerotic nano-hemodynamics has been recently examined by Nematollahzadeh et al.[21]. The main influence on the deteriorated blood-flow profile was taken to be due to a significant fibrofatty plaque deposition in a coronary artery. It was suspected that fluctuations in the blood pressure-drop could be attributed at least to four controlling factors. It was speculated that the

same four factors could directly influence blood viscosity, too. Blood was assumed to obey the classical Herschel-Bulkley model. The biofluid properties were to be tracked down by combining the physics of an assumed plug flow (along the flow centerline) and a Poiseuille flow (adjacent to the arterial wall surface). The inherent narrowing of the flow cross-section due to the fibrofatty plaque obstruction was bound to complicate the hemodynamics. Thus, a departure from a condition of a normal blood flow was clearly anticipated[22]. When experimenting with blood-viscosity models, the yield stress term may also introduce significant uncertainty in the overall non-Newtonian flow predictions. This is because the local wall topology attenuates the fluid mechanics to its proximity [23]. Owing to noise from multifarious sources, profiling effects from blood flow data becomes itself a complex process. At the core of modeling the abnormal behavior of atherosclerotic nano-hemodynamics might be the robust quantification of the uncertainty and its potential asymmetric influence at different controlling factor settings [24, 25].

One commonly-used toolset in the robust optimization of biotechnological products/processes is associated with the Taguchi method[26]. Taguchi's quality improvement philosophy requires organizing rapid and economic trials in order to swiftly gain knowledge on the researched product/process tendencies[27]. It often promotes the synchronous stochastic screening and parameter optimization for a group of investigated effects. Enquiring the optimum for a process/product performance does not mean that experiments should be executed in isolation from its real production environment. Moreover, product performance is adjusted taking in account its pragmatic conditions of use. There is a plethora of paradigms of successful applications of the Taguchi method that extends to knowledge discovery in chemical systems and other innovative products[28]. One such contemporary application of the Taguchi

method has been focused on the bioengineered nano-regulation of the atherosclerotic hemodynamics[21]. In that study, the blood pressure drop was the critical characteristic that it was sought to be optimized; it was symbolized as: -dp/dz (Pa/m). Four controlling factors were considered for that study: 1) the radius of the smallest coronary-artery cross-section area, owing to the artery narrowing which is caused by the deposited fibrofatty plaque, R (m), 2) the iron-oxide (Fe_3O_4) nano-particle volume-fraction, ϕ (%), 3) the initial velocity of the blood, V_o (m/s), and 4) the blood behavior index[1], n. The investigation implemented a four-level, four-factor $L_{16}(4^4)$ Taguchi-type orthogonal array (OA) to accommodate the four examined controlling factors. The experimental design was balanced, unreplicated but not saturated. There was a provision to allocate remainder degrees of freedom such that to estimate the experimental error. The four-level trial plan was selected in order to ensure that if there are any non-linear effects among the four examined controlling factors, then, it will be likely to uncover their curvature(s). Usually, a three-level OA is minimally recommended to track unknown non-linear effect trends, but the four-level design heightens the resolution for a discovery. Of course, ramping up the number of tested factor levels increases the total number of required trials and consequently its project cost. No prescreening of the effects was conducted. Thus, it was attempted to be simultaneously captured in a single step: 1) the effect potency, 2) the effect curvature, and 3) the effect optimization - as envisaged through the classical Taguchi experimentation philosophy. There is merit in this strategy because it signifies a substantial acceleration of the discovery process by greatly reducing the total trial logistics. This makes practical and economic sense when viewing it from a wider engineering perspective[27]. Nevertheless, a task that engages stochastic screening/optimization tools to a targeted complex

product/process cannot be reliable if ensuing asymmetric manifestations of the experimental uncertainty, among the different tested trial recipes, are not contained [29, 30]. Blood flow may be viewed as a multi-component chemical system but also as a complex biological system that continuously interacts with other intricate physiological systems. Non-linearity and non-normality may not be exempted from the basic framework of modeling abnormal blood pressure behavior. Thus, any attempt to reasonably predict fluctuations in the blood flow properties should be capable of distinguishing between the signal and the noise contributions. To achieve this, a seamless coordination of an effective data collection scheme with a robust data analysis strategy is desired. A Taguchi-type sampling strategy is usually efficient if measurements are replicated such that the signal to noise ratio can be evaluated among replicates. For unreplicated trials, the signal to noise ratio can still be established but its usage ceases to be meaningful as a preferred variability estimator[31]. But uncertainty always lurks in experiments and it is immaterial if the trials have been programmed with Taguchi-type orthogonal recipes. Optimal predictions, which have been estimated from measurements, to be viable still require a convincing disjunction of the signal from the noise[32]. In dense unreplicated Taguchi-type trials, it is probably more pertinent to ensure the symmetric contribution of uncertainty across all conducted recipes before reaching to any statistical inferences [33]. In modeling pathological blood flow characteristics this aspect may become pivotal because of the intermixing of multi-natured distributions, i.e. often dictated from various sporadically altering conditions. The resulting nonreplicated messy datasets would necessitate a proper analysis tactic that focuses on the restricted data volume that is available [34, 35]. Messiness in gathered data is not foreign to chemical engineering studies as non-Gaussian phenomena, data

inconsistencies and model inadequacies may run rampant in complex chemical systems [36, 37]. Orthogonally-designed Taguchi-type experiments when paired with a robust analysis that is apt to handle fast, dense, and messy datasets perhaps might find more often application opportunities in the field of stochastic screening/optimization of complicated chemical processes. Areas such as screening complex reaction networks, optimizing biomedical processes as well as large-size industrial operations may be benefited, too [38-40]. Fast and robust profilers have already been contrived to diagnose non-linear effects in small and messy datasets for polymerase chain reaction processes[41]. The purpose of this work is to review an iron-oxide nano-particle screening-optimization (dual) process in an atherosclerotic coronary artery by re-working from a different perspective the blood pressure-drop datasets of Nematollahzadeh et al. [21]. The major motivation for focusing on this bio-chemical system is because ischemic heart disease and stroke is the world's primary causes of human deaths[45]. Worldwide deaths which have been attributed to both diseases tallied up to 15.2 million in the year 2016 alone. Naturally, it is bound to attract great scientific attention. The cardiovascular disease is associated with impaired blood circulation in the heart vessels due to the excessive fibrofatty plaque depositions. Plaque formation restricts blood flow in the heart muscle and thus it causes oxygen delivery rate to decrease. Elevated blood pressure levels that persist over time may signal the onset and development of pathological conditions owing to atherosclerosis. Similarly, ischemic stroke occurs when brain arteries become very narrow, such as in the case of an advanced-stage atherosclerosis, leading to severely reduced blood-flow toward the brain cells. Atherothrombogenesis exacerbates further the fatality probability because the fat and cholesterol plaque buildup in the artery walls may rupture, thus triggering a blood clot

formation. Therefore, the study of the phenomena that cause such progressive physiological deterioration may aid to gaining knowledge such as to prevent future health impairment. Ostensibly, examining further the effect properties in the atherosclerotic coronary-artery flow data, published by Nematollahzadeh et al. [21], merits the additional effort because it exemplifies a pathological blood-flow improvement research that is first in its kind in the current scientific literature. A methodological section follows where the robust screening/optimization essentials for a fast and robust analysis are described. Extensive analysis of the case study is detailed in the Results section along with issues that may be raised from the implementation of alternative techniques in the Discussion section. Conclusions summarize the importance of our findings and suggestions for future work. The paper is organized in a manner that emphasizes the empirical case study as the centerpiece for the research effort rather than focusing on a general development of a theory that may be didactic but lacks immediate practical/engineering application[42].

2. Methodology

2.1 The basic hemodynamic flow model

Hemorheology is a field that explores the non-Newtonian behavior of the blood flow. Blood is a shear thinning fluid. Its properties are influenced by its plasma and cell constituents. Blood viscosity is regulated by the plasma viscosity, the hematocrit level, the fluid temperature as well as physicochemical phenomena such as the erythrocyte aggregation and deformability. To evaluate the blood flow properties in an atherosclerotic coronary artery, dispersions of nano-particles were utilized, for the first time, in the recent research by Nematollahzadeh et al. [21]. Magnetite nano-particles were introduced into the blood stream in an attempt to model the

strength and significance of four specific controlling factors on the blood pressure-drop. The proposed constitutive law was based on the Herschel-Bulkley model. This rheological model selection offered the joint predictive advantages of the power-law and Bingham plastic models:

$$\tau_{rz} = \tau_o + \mu_{eb}\left(-\frac{\partial v_z}{\partial r}\right)^n \quad (1)$$

where τ_{rz} is the rz-stress tensor component in polar coordinates and τ_o is the yield stress. Moreover, the quantity v_z is the velocity component in the z-direction and n is the blood behavior index which specifies the extent of the non-Newtonian blood behavior as controlled by several constituents such as cholesterol, hematocrit, fibrinogen and so forth. The blood behavior index is fitted from viscosity data collected from standard viscometers. The effective blood viscosity, μ_{eb}, was defined as:

$$\mu_{eb} = \left(\frac{1+a\varphi^2+b\varphi^4}{1+c\varphi^2+d\varphi^4}\right)\mu_b \quad (2)$$

where φ is the volume fraction of the magnetite (Fe_3O_4) nano-particles in the blood stream. It is estimated from the masses and densities of the two added materials. The fitted coefficients were found to be: a = 0.13, b =2.24, c =0.13, d =1.91. The viscosity of blood, μ_b, was defined as:

$$\mu_b = \mu_p(1 + 0.025H + 7.35 \times 10^{-4}H^2) \quad (3)$$

with average hematocrit value, H, of 40 and blood plasma viscosity value, μ_p, of 1.10 mPa·s at 37 ^{o}C. The effective density of the blood fluid, ρ_{eb}, was estimated from the blood density, ρ_b (=1060 kg m^{-3}), and the nano-particle density, ρ_{np} (=5.17 kg m^{-3}), through the volume fraction of the particles in the equation:

$$\rho_{eb} = \rho_b(1-\varphi) + \varphi\rho_{np} \tag{4}$$

The equations of motion were solved using the Herschel-Bulkley model (eq. 1) in a narrow tube geometry while allowing for the possibility of a tilted arterial-vessel topology at an angle, β. The final quantity of interest that was derived by Nematollahzadeh et al. [21] is the blood pressure-drop expression that was found to be:

$$-\frac{dp}{dz} = \frac{2\mu_{eb}\left(\frac{R_o}{R(z)}\right)^{2n} v_o^n}{\left(R(z)-r_{pf}\right)^{n+1}} \times \left[\frac{\frac{(n+1)(1+2n)(1+3n)}{n}}{(1+n)(1+2n)+2n(1+n)\left(\frac{r_{pf}}{R(z)}\right)+2n^2\left(\frac{r_{pf}}{R(z)}\right)^2}\right]^n - \rho_{eb}gsin(\beta) \tag{5}$$

In equation 5, the effective tube radius, $R(z)$, is attributed to the fibrofatty vessel-wall deposits, and the initial blood velocity, v_o. Also, the plug flow radius, r_{pf}, was defined as:

$$r_{pf} = \frac{2\tau_o}{-\frac{dp}{dz} + \rho_{eb}gsin(\beta)} \tag{6}$$

2.2 The effect screening method

Effect screening and parameter optimization are traditionally treated as two separate optimization stages that complement innovation, discovery and improvement projects [27, 28, 31]. Effect screening is the less visible procedure of the two as its direct connection to optimization is rarely acknowledged. However, effect screening is a crucial optimization step, inasmuch as

during this stage, the strength hierarchy of a group of investigated factors is stochastically gauged. The end deliverable is a minimized (short) list of factors that will receive a deeper probing in the next stage where the parameter optimization is to be undertaken. Therefore, the primary goal of screening is the elimination of weak-performing effects. Criteria, based on economic and/or other practical considerations, are often imposed on the stringent requirements of industrial experiments. To be meaningfully exploitable, the conduction of industrial trials necessitates the actual utilization of operational machinery and other line equipment units. A common specification is that trials ought to be carried out rapidly with minimum schedule interruptions and minimum resource usage. A similar philosophy may be applied to studies that focus on blood biomedical engineering. Hemorheologically-related variables are expected to exhibit non-linear dependencies - according to eqs 1-6. Then, a methodology for stochastic screening/optimization should incorporate information from the individual strength as well as the type of curvature of the investigated effect. The basic tactic is to use the practical rule of minimum trials that could allow deciphering a statistically estimated trend. This might be accomplished by either implementing a three- or four-setting Taguchi-type orthogonal array (OA) in order to plan the experiments. In bio-modeling a non-linear blood-flow condition, a four-level OA may seem to be preferable because it provides the minimum opportunity to reveal skewed behavior in the data. On the other hand, comparing to selecting a corresponding three-level OA, a four-level OA is more expensive to carry out since it requires more trials. Nematollahzadeh et al. [21] adopted the same industrial experimentation mentality to screen and optimize the behavior of a very difficult process, that of the reduction of the atherosclerotic coronary blood pressure. Strictly from an engineering design point of view, an

$L_9(3^4)$ OA could have been implemented to accommodate all four nominated factors and would simultaneously allow the tracing of any non-linear modulations if befitting (Table 1). Such choice would maximize the number of permitted factors that the trial plan could exploit, which coincides with the desired group size of four. It also minimizes the number of experimental recipes that need to be formulated to just nine. A single execution of the resulting nine OA recipes would evoke the "unreplicated and saturated" constraint on the screening dataset. This type of data structure deters standard multifactorial solvers from reaching to a trustworthy prediction because all available degrees of freedom are reserved to be distributed only among the studied effects. Hence, no remainder is allowed for an estimation of the experimental error [31, 41]. Even though there are specialized methods to overcome this complication, Nematollahzadeh et al. [21] opted for the $L_{16}(4^4)$ OA design (Table 1) that upfront disposes of this condition by reserving at least three degrees of freedom for estimating the unexplainable error. Another obvious advantage of such a decision is that two middle factor settings, instead of one as in the $L_9(3^4)$ OA option, are allocated to ensure the detection of a non-linear effect by probing the shape of the curvature through four increasing control adjustments. Both of those propitious features mount up to an increase of 78% in the sampling requirement – from nine to sixteen recipes - when compared to the alternative $L_9(3^4)$ OA plan. Of course, now, the design structure is relieved from the "saturated" OA condition but it still retains the "unreplicated" form. Unreplication is not necessarily an alarming restriction in engineering trials since resource savings are always to be realized. Thus, it may be viewed as a favorable condition as long as the quantification of uncertainty is coped with.

The original $L_{16}(4^4)$ OA dataset of Nematollahzadeh et al.[21] along with the logarithmic transformation of the response gradient –(dp/dz) data have been tabulated in Table 2. The non-linear surrogate screening/optimization method of Besseris[31] is used to decompose the compacted blood pressure-drop response. The general method, which might be applicable for any type of a non-linear multifactorial problem, has been outlined in Besseris[31] along with an illustrative example from the biomedical area of screening/optimization of a polymerase chain reaction process. That highlighted paradigm involved an unreplicated $L_9(3^4)$ OA design. Therefore, the procedure of setting up a $L_9(3^4)$ OA-designed dataset for analysis will not be repeated in this work.

Table 1: Four-factor non-linear OA plan options.

$L_9(3^4)$ OA						$L_{16}(4^4)$ OA				
	Factors						**Factors**			
Run #	**A**	**B**	**C**	**D**		**Run #**	**A**	**B**	**C**	**D**
1	1	1	1	1		**1**	1	1	1	1
2	1	2	2	2		**2**	1	2	2	2
3	1	3	3	3		**3**	1	3	3	3
4	2	1	2	3	→	**4**	1	4	4	4
5	2	2	3	1		**5**	2	1	2	3
6	2	3	1	2		**6**	2	2	1	4
7	3	1	3	2		**7**	2	3	4	1
8	3	2	1	3		**8**	2	4	3	2
9	3	3	2	1		**9**	3	1	3	4
						10	3	2	4	3
						11	3	3	1	2
						12	3	4	2	1
						13	4	1	4	2
						14	4	2	3	1
						15	4	3	2	4
						16	4	4	1	3

Table 2: The original nano-regulated atherosclerotic blood pressure-drop response[21].

Run #	R	V_o	N	ϕ	-(dp/dx)	Ln(-(dp/dx))
1	0.0015	0.25	0.5	0	141.37	4.951381
2	0.0015	0.3	0.78	0.5	1018.01	6.925605
3	0.0015	0.35	1	1.5	5491.89	8.611028
4	0.0015	0.4	1.5	2	175287.10	12.07418
5	0.0012	0.25	0.78	1.5	2090.95	7.645374
6	0.0012	0.3	0.5	2	325.02	5.783887
7	0.0012	0.35	1.5	0	398468.66	12.89538
8	0.0012	0.4	1	0.5	13590.51	9.517127
9	0.00105	0.25	1	2	15928.14	9.675843
10	0.00105	0.3	1.5	1.5	829928.90	13.6291
11	0.00105	0.35	0.5	0.5	444.04	6.095915
12	0.00105	0.4	0.78	0	3736.63	8.225939
13	0.0009	0.25	1.5	0.5	1308082.66	14.08407
14	0.0009	0.3	1	0	28818.44	10.26877
15	0.0009	0.35	0.78	2	6914.90	8.841434
16	0.0009	0.4	0.5	1.5	780.61	6.660076

The non-linear surrogate screening/optimization method is fairly new and novel since the only other application that has been attempted is in a demanding manufacturing process[46] where a four-level $L_{16}(4^4)$ OA was utilized.

The general steps of the methodology for the screening-optimization task are:

1) Select and prepare the response datasets for the appropriate four-level OA arrangement.
2) Evaluate the robust micro-analytics per investigated controlling factor, i.e. use the estimators: median, interquartile range (IQR), skewness, excess kurtosis.

3) Inspect the main effects plots for the raw responses as well as for the log-transformed entries.
4) Assess curvature tendencies and goodness of fit using the general linear modeling approach.
5) Inspect effect-shape anisotropies using boxplots in the original and in the log-transformed dataset versions.
6) Evaluate uncertainty and effect symmetries within the various controlling factor settings using the non-linear surrogate profiling method.
7) Decide on the stochastically strong effects and suggest the optimal settings.
8) Assess and demonstrate the possibility of transferring the data generation process to smaller, i.e. to more economic and faster OA designs, for more practical trial deployment and quicker decision-making.

2.3 The effect screening model analysis for the $L_{16}(4^4)$ OA.

To simplify the dataset layout form for the analysis part that follows, we define the response variable, y, which is meant to be pertinent for either of the two data types that we choose to work with, i.e.:

$$y = \left\{-\frac{dp}{dz}\right\} \text{ or } y = \left\{Ln\left(-\frac{dp}{dz}\right)\right\} \quad (7)$$

The generic non-linear effects model for four four-level tested effects that are symbolized as A, B, C and D will be:

$$y_{\alpha\beta\gamma\delta} = M + A_\alpha + B_\beta + C_\gamma + D_\delta + \varepsilon_{\alpha\beta\gamma\delta} \tag{8}$$

Each of the subscripts, α, β, γ, and δ in equation 8 mirrors the four admissible states appointed by each respective recipe as dictated by the $L_{16}(4^4)$ OA in Table 1. It is generically coded as: α_i, β_j, γ_k, and δ_l, $\forall$ $i, j, k, l \in \{1, 2, 3, 4\}$. By default, we let coded levels '1' and '4' to represent the two selected operating endpoints of each factor. No assumptions are placed on the error term, $\varepsilon_{\alpha\beta\gamma\delta}$. Simply, it should be checked for stochastic symmetry across the four settings, for each examined factor individually. This checking should be completed before attempting to assess the results of the effect screening/optimization task. The overall (grand) median, M, for all *16* $y_{\alpha\beta\gamma\delta}$ response entries is defined as:

$$M = \text{med}\left(\{y_{\alpha\beta\gamma\delta}\}\right) \tag{9}$$

The four factorial contributions of the terms in equation 8 may be conveniently defined:

$$\begin{aligned} A_\alpha &= med_\alpha\left(\{y_{\alpha\beta\gamma\delta}\}\right) - M \\ B_\beta &= med_\beta\left(\{y_{\alpha\beta\gamma\delta}\}\right) - M \\ C_\gamma &= med_\gamma\left(\{y_{\alpha\beta\gamma\delta}\}\right) - M \\ D_\delta &= med_\delta\left(\{y_{\alpha\beta\gamma\delta}\}\right) - M \end{aligned} \tag{10}$$

The reconstructed response carrying the individual factorial profile is redefined as y'_x where $x \in \{\alpha, \beta, \gamma, \delta\}$.

$$\begin{aligned} y'_\alpha &= M + A_\alpha + \varepsilon_{\alpha\beta\gamma\delta} \\ y'_\beta &= M + B_\beta + \varepsilon_{\alpha\beta\gamma\delta} \\ y'_\gamma &= M + C_\gamma + \varepsilon_{\alpha\beta\gamma\delta} \\ y'_\delta &= M + D_\delta + \varepsilon_{\alpha\beta\gamma\delta} \end{aligned} \tag{11}$$

For each effect separately, we rank-order y'_x which leads to the rank response, r_x :

$$y'_x \rightarrow r_x \text{ where } x = \alpha, \beta, \gamma \text{ or } \delta \quad (12)$$

Mean rank sums of the four data entries for each factor-setting are formed according to the prescription of the Kruskal-Wallis method[31, 43].

$$\bar{R}_{x_i} = \frac{\sum_{x_i} r_{x_i}}{4} \text{ where factor } x \in \{\alpha, \beta, \gamma, \delta\} \text{ and level } i \in \{1, 2, 3, 4\} \quad (13)$$

The Kruskal-Wallis test statistic[31], H_x, is appropriate for testing the one-way fluctuation of ranks across the four settings for a total of n=16 observations:

$$H_x = \frac{3}{17}\sum_{i=1}^{4} \bar{R}_{x_i}{}^2 - 51 \text{ where factor } x \in \{\alpha, \beta, \gamma, \delta\} \quad (14)$$

The stochastic validity of equation 14 hinges upon demonstrating the uniformity and stability of the residual error. This uncertainty component is constructed from the fragmentation of the response while retaining only the part that relates to the residual error for each specific recipe. The uncertainty vector is y'' such that:

$$y'' = M + \varepsilon_{\alpha\beta\gamma\delta} \quad (15)$$

Repeating the rank-ordering process for y'', this time will yield the transformed uncertainty response, r':

$$y'' \rightarrow r' \quad (16)$$

Forming the mean rank sums of the r' variable for each four setting entries, we obtain for each individual factor setting, $\bar{R}'_{x_i}$:

$$\bar{R}'_{x_i} = \frac{\sum_i r'_{x_i}}{4} \text{ where factor } x \in \{\alpha, \beta, \gamma, \delta\} \text{ and level } i \in \{1, 2, 3, 4\} \quad (17)$$

The Kruskal-Wallis test statistic for testing symmetry across the recipe uncertainties, H_{ux}, is similarly defined as:

$$H_{ux} = \frac{3}{17}\sum_{i=1}^{4} \bar{R}'^{\,2}_{x_i} - 51 \text{ where factor } x \in \{\alpha, \beta, \gamma, \delta\} \quad (18)$$

The exact Kruskal-Wallis-test significance values for equations 14 and 18 are computed with the statistical software package STATISTICA 9 (StatSoft). The significance of the stochastic comparisons in equation 14 may be reliable as long as there is no detected statistical significance which is attributed to uncertainty fluctuations across all four settings for each controlling factor separately (equation 18). Results are finalized after rating significances by controlling the false discovery rate for the multi-factorial treatment[44].

3. Results

In Table 3, we have tabulated the respective micro-analytics, i.e. median, IQR, skewness, and excess kurtosis estimations (MINITAB 18) for the hemodynamical pressure-drop datasets of Table 2. The descriptive trends have been evaluated for both the original dataset as well as the log-transformed response. It is obvious that the blood index behavior dramatically regulates the variability of the pressure-drop magnitude regardless of the dataset form. The rise of the setting median values of the pressure-drop due to n transcends to three orders of magnitude. From a design engineering standpoint, the corresponding IQR behavior of the pressure drop is also modulated by tweaking n. The pressure drop does not seem to react to varying the rest of the screened factors.

Table 3: Descriptive robust micro-analytics of the four factors of the blood pressure-drop.

Micro-analytics for:	R vs	-(dp/dz)		R vs	Ln(-dp/dz)	
Variable	**R**	**Total Count**	**Median**	**IQR**	**Skewness**	**Excess Kurtosis**
–(dp/dz)	0.0009	4	17867	985952	2	3.99
	0.00105	4	9832	625162	2	3.99
	0.0012	4	7841	301483	1.99	3.98
	0.0015	4	3255	132478	2	3.99
Ln(-(dp/dz))	0.0009	4	9.56	5.92	0.71	0.85
	0.00105	4	8.95	6.01	0.78	0.92
	0.0012	4	8.58	5.8	0.64	0.06
	0.0015	4	7.77	5.76	0.65	0.35

Micro-analytics for:	V_o vs	-(dp/dz)		V_o vs	Ln(-dp/dz)	
Variable	**V_o**	**Total Count**	**Median**	**IQR**	**Skewness**	**Excess Kurtosis**
–(dp/dz)	0.25	4	9010	984415	2	4
	0.3	4	14918	629153	1.99	3.98
	0.35	4	6203	298874	2	4
	0.4	4	8664	133343	1.98	3.91
Ln(-(dp/dz))	0.25	4	8.66	7.36	0.59	0.44
	0.3	4	8.6	6.72	0.63	-1.68
	0.35	4	8.73	5.16	0.8	1.83
	0.4	4	8.87	4.38	0.57	0.25

Micro-analytics for:	n vs	-(dp/dz)		n vs	Ln(-dp/dz)	
Variable	**n**	**Total Count**	**Median**	**IQR**	**Skewness**	**Excess Kurtosis**
–(dp/dz)	0.5	4	385	509	0.77	0.97
	0.78	4	2914	4834	0.99	0.47
	1	4	14759	18079	0.71	1.51
	1.5	4	614199	957462	0.56	-1.36
Ln(-(dp/dz))	0.5	4	5.94	1.36	-0.52	0.76
	0.78	4	7.936	1.582	-0.16	-0.78
	1	4	9.596	1.283	-0.66	1.49
	1.5	4	13.262	1.691	-0.47	-1.31

Micro-analytics for:	ϕ vs	-(dp/dz)	ϕ vs	Ln(-dp/dz)		
Variable	**ϕ**	**Total Count**	**Median**	**IQR**	**Skewness**	**Excess Kurtosis**
–(dp/dz)	0	4	16278	305016	1.97	3.91
	0.5	4	7304	983872	2	4
	1.5	4	3791	622711	2	4
	2	4	11422	133475	1.97	3.88
Ln(-(dp/dz))	0	4	9.25	6.47	-0.25	-0.19
	0.5	4	8.22	6.64	1.15	0.53
	1.5	4	8.13	5.47	1.61	2.76
	2	4	9.26	4.93	-0.37	1.08

Data messiness may be contemplated at this stage as a complicating condition. One way that it may be quickly construed is by inspecting the magnitudes of the estimations of the effects through the measures of skewness and excess kurtosis in Table 3. In brief, an intermixing of conflicting tendencies is manifested as follows:

a) *For the original data:* There is a consistent departure from normality in accord to all skewness estimates. Skewness values for all examined settings of R, V_o and ϕ are in the vicinity of '+2' which implies that their distributions are consistently highly skewed on the right. All settings for n are also skewed right to a lesser degree though. Furthermore, there is a departure from normality according to an assessment on the excess kurtosis estimations. All settings of R, V_o and ϕ are leptokurtic. The peakedness of the settings of n is milder leptokurtic and on its highest adjustment (n=1.5) switches to platykurtic (<0).

b) *For the transformed data*: In general, a departure from normality is detected in the skewness estimates but it appears to be moderate for all factors. This is compatible to the impact of a log-transformation on the dataset distribution. For all the settings of R and V_o, the setting distributions are skewed right. Setting distributions due to n are

skewed left. The ϕ-factor settings display mixed tendencies with setting distributions to alternate skewness directions. Excess kurtosis estimations are overall less diverted from normality in contrast to the original dataset. Three of the four factors exhibit an intertwined trend by mixing leptokurtic and platykurtic behavior.

c) From comments in a) and b) above, it is plausible to proceed by separately conducting screening/optimization predictions for the two different data types and then compare their outcomes for some level of agreement.

Depicting the appropriate main effects plots is always advisable as a preliminary screening step. The two response graphs (MINITAB 18) that portray the four effects on the blood pressure-drop are prepared in terms of the original dataset (Fig. 1A) and in its log-transformed response version (Fig. 1B). From either plot, we deduce that the blood behavior index is again the dominant effect, at least in a qualitative way. However, the initial velocity and the nano-particle volume fraction appear to possess conflicting relative strengths, which depend on the data type we opt to treat the pressure-drop response. For example, in Fig. 1A, both of those two controlling factors could influence the characteristic behavior of the blood pressure in spite of exhibiting distinctly different curvature trends. On the contrary, when the blood pressure drop data have been log-transformed (Fig. 1B), then both of those factors may be clearly declared as inactive. Finally, sizing the effect of the radius of the atherosclerotic coronary artery, R, we may surmise that it causes some detectable disturbance in both kinds of screenings. But its relative effect with respect to the blood behavior index varies between the two screenings. To cast the potencies of the four controlling factors in a functional form, we fit the dataset of Table 2 in both versions by employing the General Linear Modelling method (MINITAB 18).

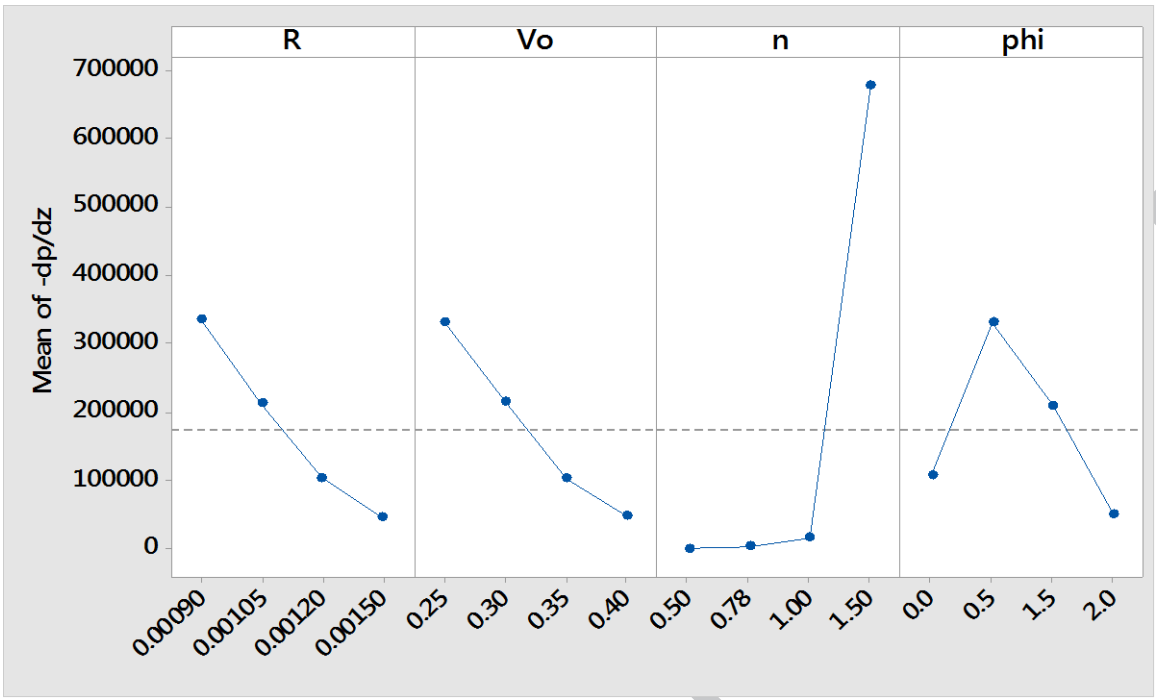

A)

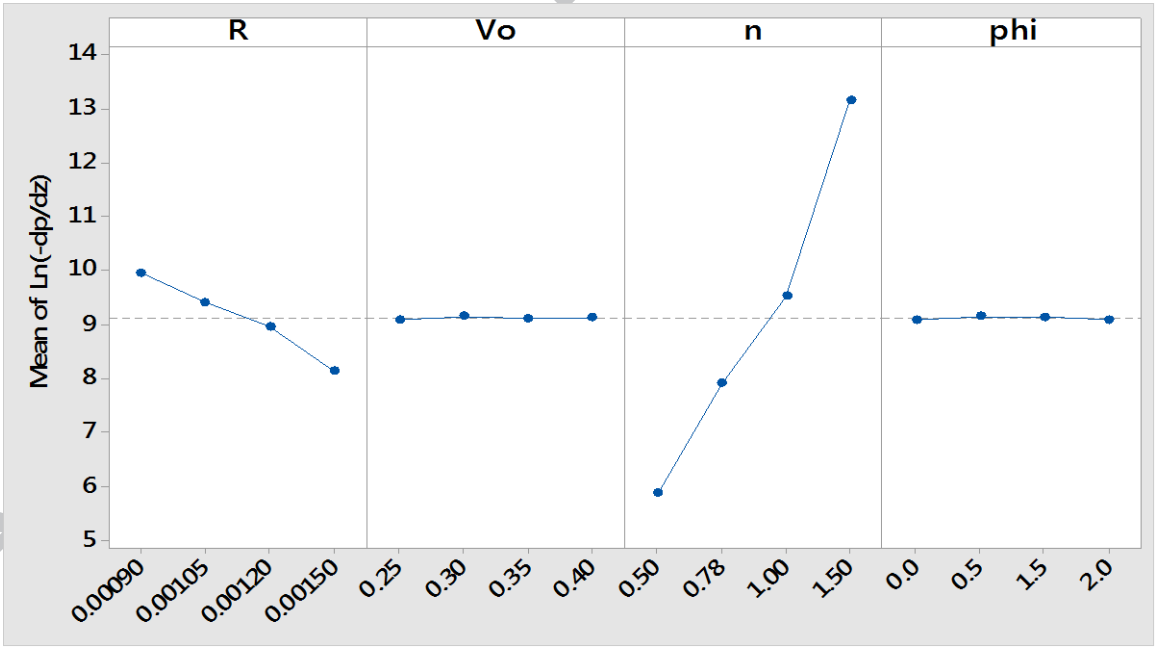

B)

Figure 1: Main effects plot for the blood pressure-drop: A) –(dp/dz), and B) Ln(-(dp/dz)).

Table 4: General Linear Modelling of the blood pressure drop in the original (A) and transformed (B) data.

	A: Original Data					*B: Log-transformed Data*			
Term	**Coef***	**SE Coef**	**T-Value**	**P-Value**		**Coef****	**SE Coef**	**T-Value**	**P-Value**
Constant	-2.15E6	3.50E7	-0.06	0.955		5.2	29.6	0.17	0.873
R	3.22E9	6.61E10	0.05	0.964		-1.90E4	5.59E4	-0.34	0.756
V_o	1.62E7	2.30E8	0.07	0.948		67	194	0.35	0.752
n	2.68E6	9.73E6	0.28	0.801		7.04	8.24	0.85	0.456
ϕ	7.27E5	6.52E5	1.11	0.346		0.217	0.552	0.39	0.720
R^2	-4.16E12	5.68E13	-0.07	0.946		1.25E7	4.81E7	0.26	0.811
V_o^2	-6.32E7	7.16E8	-0.09	0.935		-204	607	-0.34	0.759
n^2	-3.71E6	1.08E7	-0.34	0.754		0.27	9.16	0.03	0.978
ϕ^2	-6.24E5	7.96E5	-0.78	0.490		-0.169	0.674	-0.25	0.818
R^3	1.42E15	1.59E16	0.09	0.934		-3.20E9	1.35E10	-0.24	0.828
V_o^3	7.12E7	7.34E8	0.10	0.929		204	622	0.33	0.765
n^3	1.67E6	3.69E6	0.45	0.682		-0.08	3.12	-0.03	0.980
ϕ^3	1.23E5	2.60E5	0.47	0.668		0.031	0.220	0.14	0.896

Regression Equations:

$$*\text{-dp/dz} = -2151139 + 3216713083\,R + 16225141\,V_o + 2677576\,n + 727172\,\phi - 4160014361111\,R^2 - 63170218\,V_o^2 - 3709853\,n^2 - 623789\,\phi^2 + 1424689444444458\,R^3 + 71154790\,V_o^3 + 1667584\,n^3 + 122829\,\phi^3 \quad (19)$$

$$**\text{Ln(-pd/dz)} = 5.2 - 19022\,R + 67\,V_o + 7.04\,n + 0.217\,\phi + 12542057\,R^2 - 204\,V_o^2 + 0.27\,n^2 - 0.169\,\phi^2 - 3201110158\,R^3 + 204\,V_o^3 - 0.08\,n^3 + 0.031\,\phi^3 \quad (20)$$

Model Summary

Response	R^2	R^2(adj)	R^2(pred)
-(dp/dz)	91.35%	56.74%	0.00%
Ln(-(dp/dz))	99.89%	99.46%	96.95%

The four-level $L_{16}(4^4)$ OA design allows regression-fitting of the linear, quadratic and cubic terms of all four controlling factors. We list the respective coefficients for each factor in Table 4 as well their model building strength contribution and significance. From Table 4, we infer that no effect is significant according to the processing of the original dataset.

Not even the constant term can be stabilized at level of significance of 0.05. However, its coefficient of determination, R^2, which demonstrates the goodness of the curve fitting, is estimated at 91.35%. The corresponding predicted R^2 estimation dips to 0% to no avail. On the other hand, the modeling of the log-transformed dataset presents a substantially different picture. The regular and the predicted coefficients of determination – 99.89% versus 96.95% (model summary in Table 4B) - are not disparate from each other. Still, a constant coefficient cannot be established for this model. All four controlling factors do not play any significant role. We conclude that the predictability of detecting any active effects along with their associated curvature details becomes independent of the decision to transform or not the original blood pressure-drop dataset. Before making further inferences about the viability of both types of predictions, the residuals from both modeling efforts have been plotted in Figure 2. It is obvious that in both situations, the residuals do not obey a Gaussian reference law. This is discerned by the fact that: 1) there are points that are located on or outside the 95% confidence intervals when they are not expected to for this small sample, and 2) the Anderson-Darling test rejects - at a level of 0.05 - the normality of the residuals. We conclude that the predictions of the fitted coefficients in Table 4 may need to receive more scrutiny in order to explain more convincingly the behavior of a realistic blood pressure-drop profile under the pathological condition of atherosclerosis. This may hold for both versions of data analysis.

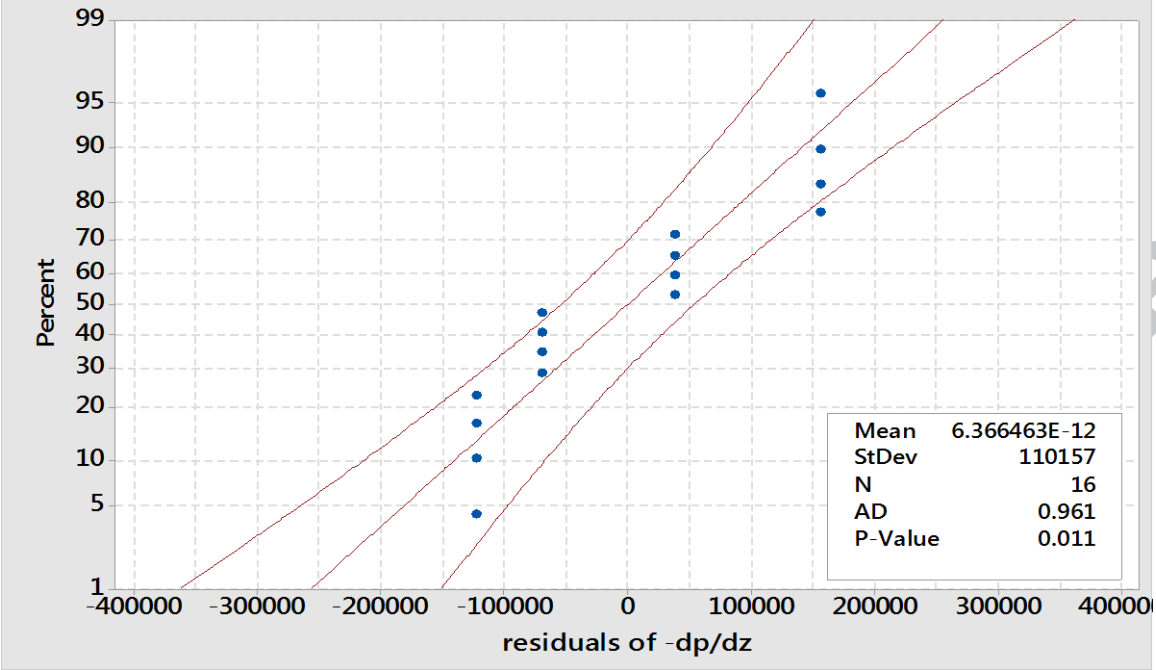

A.

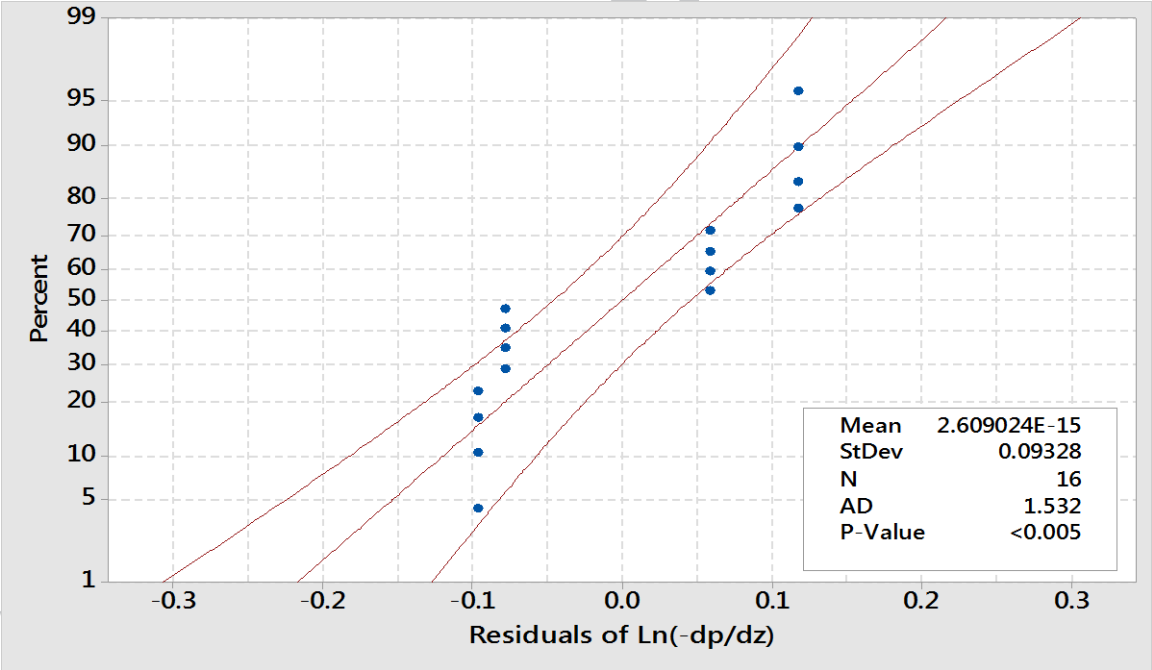

B.

Figure 2: Normal probability plots (95% confidence interval) for blood pressure drop residuals-response dataset based on: A) –(dp/dz), and B) Ln(-(dp/dz)).

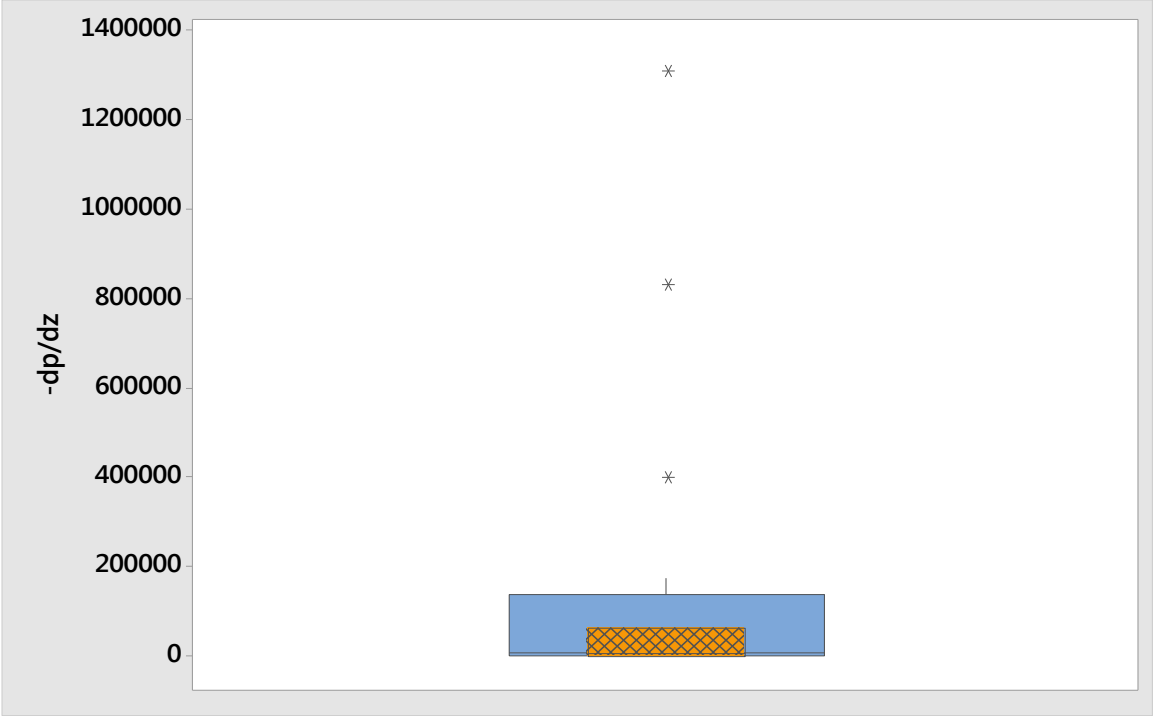

A)

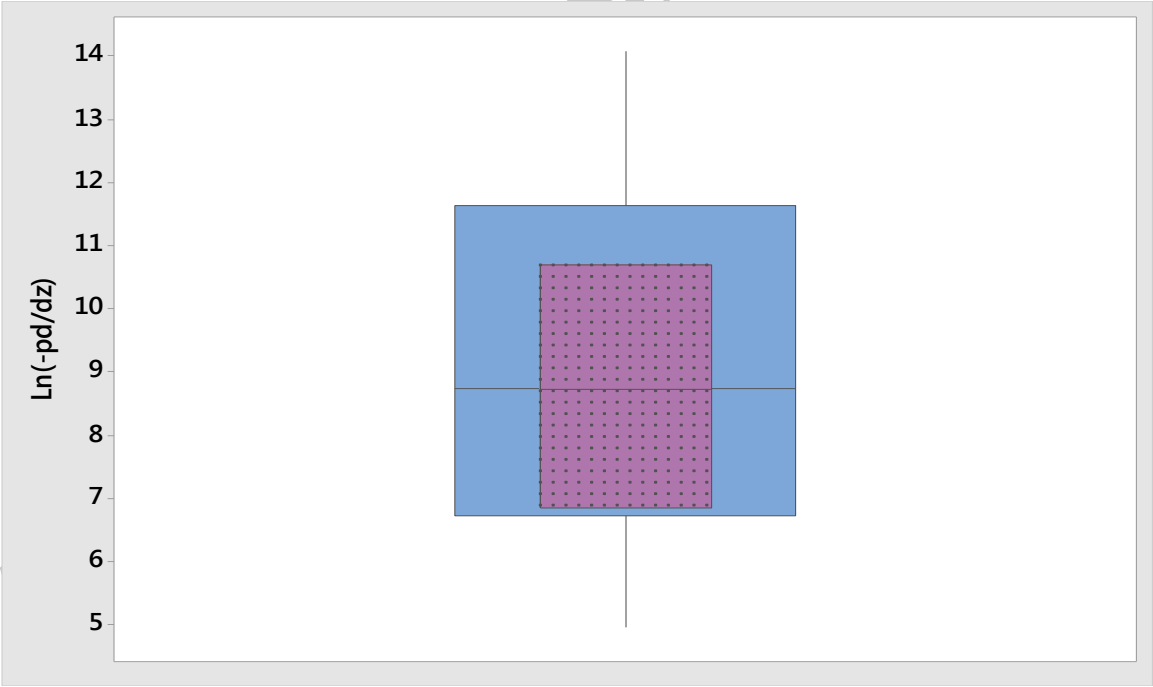

B)

Figure 3: Boxplots for the blood pressure-drop response based on: A) –(dp/dz), and B) Ln(-(dp/dz)).

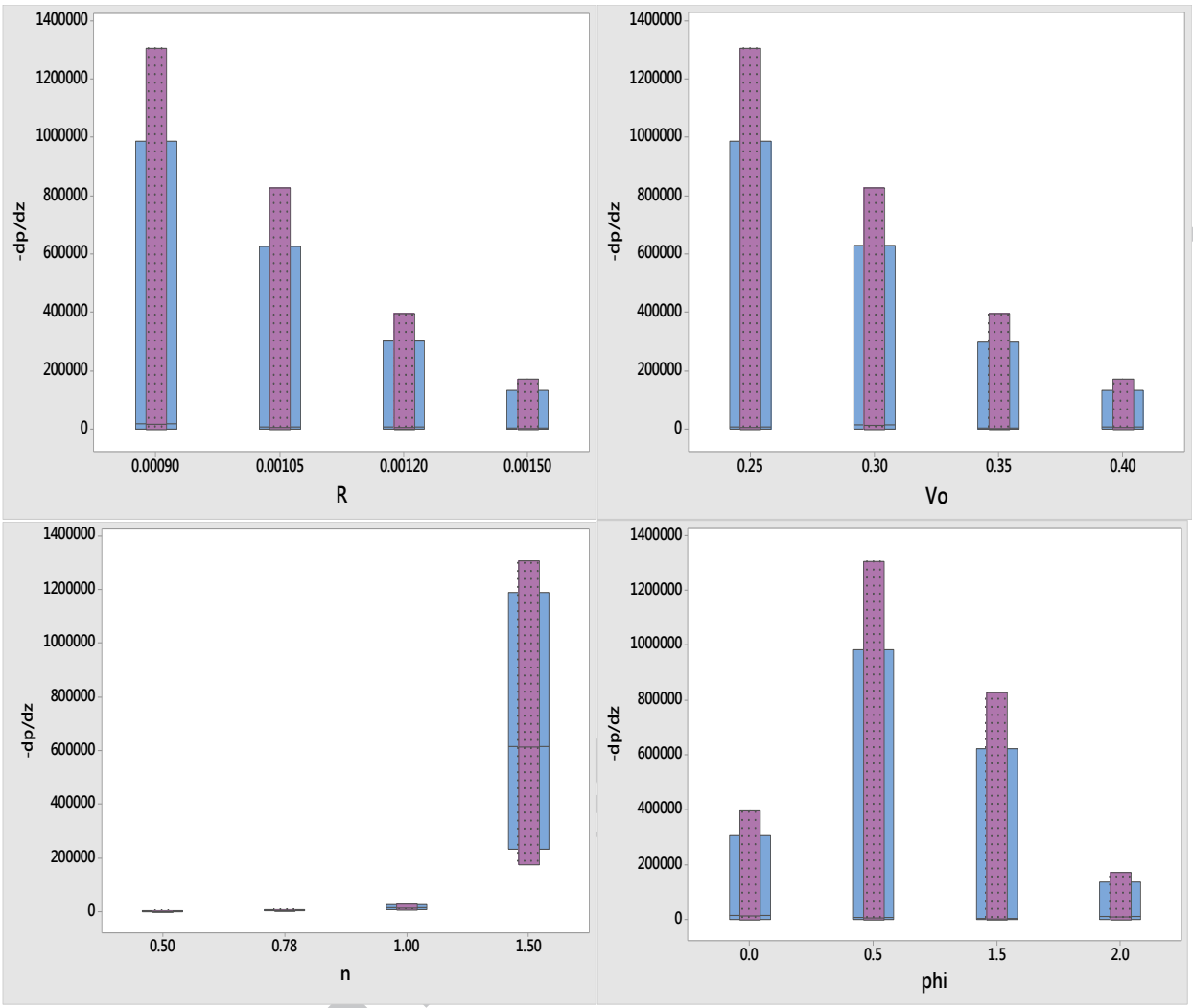

Figure 4: Boxplot screening across all factor settings for the blood pressure-drop based on the –(dp/dz) response.

At this stage, it becomes evident that the blood pressure-drop dataset of Table 2 is an interesting case study that is worthwhile to be re-investigated with a more specialized robust treatment. The overall median behaviors and the 95% confidence intervals for both types of datasets have been depicted in box-plots (Figure 3). We observe that the log-transformation of the blood pressure-drop dataset tends to favor a centered location for the median with a fairly symmetric spread of its associated bounds (Fig. 3B). In contrast, the original dataset (Fig. 3A) appears strongly skewed.

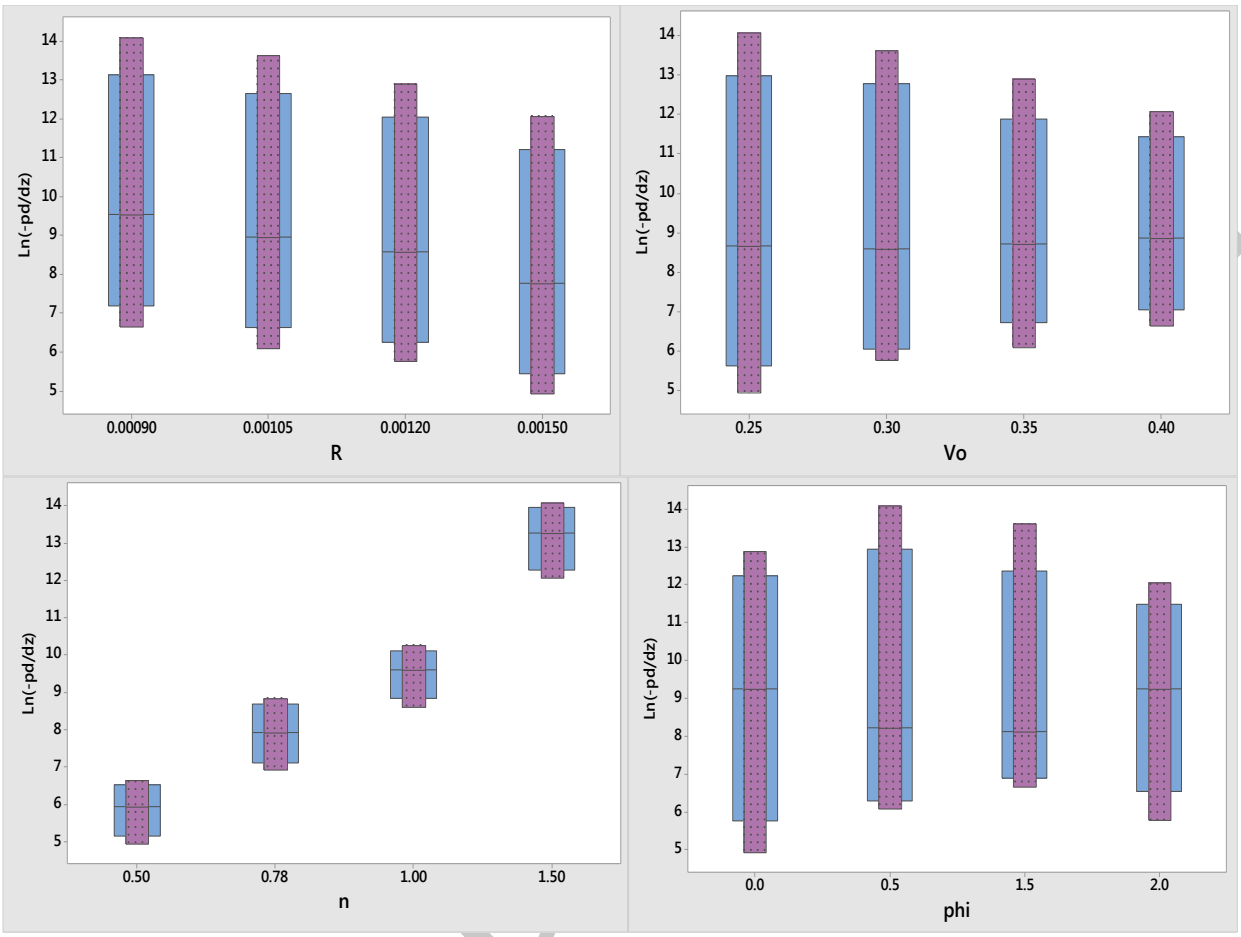

Figure 5: Boxplot screening across all factor settings for the blood pressure-drop based on the Ln(–(dp/dz)) response.

Additionally, it is remarked that the log-transformation of the data eclipses the presence of outliers and extremities that seem to distinctly protrude in the original-data boxplot (Fig. 3A). In Figure 4, the effect profiling on the –(dp/dz) gradient response reveals that there is a great non-homogeneity among different factors. There is a strong indication of severe skewness within data groups for particular settings, too. It is only the blood behavior index that influences the total response of the pressure drop. However, assessing of the outcomes from the multifactorial micro-analysis point of view should be attentive to the inherent messy-data

landscape. Key findings in the first three adjustments of the blood behavior index (Fig. 4) are: 1) no significant dispersion across settings, since all three medians are levelled, and 2) variability is very tight within each setting. On the contrary, the fourth setting (n=1.5) appears to cause a dramatic elevation on the median estimation of the –(dp/dz) gradient which is escorted with an equally dramatic increase in variability - widened 95% confidence intervals for the blood pressure-drop median predictions. We conclude that the major influence in the trials is identified to the blood behavior index. Regulating it within the range of 0.5 -1.0 will maintain the blood pressure-drop in a desirable status.

Re-examining the effects for the log-transformed data of the blood pressure-drop, we depict the tendencies of the four effects in the tiled boxplots of Figure 5. We observe that for each of the three factors, R, V_o and ϕ, there is great variability within each setting. Nevertheless, it is statistically indiscernible if we extent the comparison among the different effects. There is also a likelihood that there is some skewness in the data that is related to each of those effects. The blood pressure-drop displays an increasingly monotonic trend due to the influence of the blood behavior index. The median estimations for the four n settings are fairly balanced and their associated variability is reasonably contained. The variation of this effect transcends almost nine orders of magnitude. This descriptive micro-analysis offers a practical aid in comprehending the dominant character of the blood behavior index in connection to regulating blood pressure fluctuations in an atherosclerotic coronary-artery network. Ostensibly, it is the blood-behavior-index setting of 0.5 that will harness the hemodynamical performance in this study by maintaining the blood pressure-drop to the optimal median and IQR estimated values of 385 Pa/m and 509 Pa/m, respectively (Table 3). The optimal setting for

the blood behavior index of 0.5 improves over the natural blood rheology (n = 0.78) - with no additives - which was also represented in the experimental scheme as the second tested blood behavior index condition [1, 21]. It is insightful to review the descriptive non-parametric evaluations we discussed above from a different angle of robust micro-analytics. At this stage, a fast-and-agile multi-factorial profiler might conveniently provide value to this study by quantifying distribution-free effect significances. Utilizing our robust optimization treatment for the –(dp/dz) dataset, we list in Table 5 the nonparametric comparisons of the uncertainty balances across each individual controlling factor. This permits inspecting the symmetry of errors across all individual settings. Sizing symmetry is necessary to ascertain the stable detection of the strength of the effects. We notice the asymmetry of the experimental errors that are associated with nano-particle volume fraction, at a level of significance of 0.05. However, profiling all effects indicates that the sole active factor is the blood behavior index at a level of significance of 0.05. We repeat the same procedure for the Ln(-(dp/dz)) response and we list the outcomes in Table 6. The asymmetry of errors still persists with respect to the influence of the nano-particle volume fraction, at a level of significance of 0.05. Besides the blood behavior index that may be convincingly declared to be active, the (atherosclerotic coronary-artery) minimum cross section radius, R, may be also identified as an active factor. However, if we control the false discovery rate[44] at a significance level of 0.05, then the cross section radius is eliminated from the influential group of factors. Thus, the blood behavior index remains as the sole stochastically-predominant effect in the last robust screening effort. Consequently, all approaches that we employed in this section reach to an agreement that the

optimization of the blood pressure drop may be regulated statistically from the same single factor, n.

Table 5: Uncertainty and effect robust profiling for the –(dp/dz) dataset (Table 2).

Factor	Uncertainty		Effect	
	H	p-value	H	p-value
R	0.551	0.907	6.243	0.100
V_o	3.022	0.388	4.610	0.203
n	0.066	0.996	12.331	0.006
ϕ	9.926	0.019	2.934	0.402

Table 6: Uncertainty and effect robust profiling for the Ln(–(dp/dz)) dataset (Table 2).

Factor	Uncertainty		Effect	
	H	p-value	H	p-value
R	0.088	0.993	7.985	0.046
Vo	2.206	0.531	0.176	0.981
n	0.265	0.967	14.118	0.003
ϕ	11.338	0.010	0.860	0.835

4. Discussion

Using ordinary optimization methods to recommend nano-engineered remedies to pathological (atherosclerotic) hemodynamics may harbor arduous complications. Therefore, searching for robust techniques to predict optimal blood pressure-drop (gradient) profiles necessitated a deeper probing. First, we should stress the fact that screening and optimizing simultaneously an abnormal blood pressure-drop response using classical multi-factorials may not be applicable to all situations. Employing a more specialized method, such as the half-normal plot (Figure 6), it may still not be capable of resolving the stochastic potency of the effects.

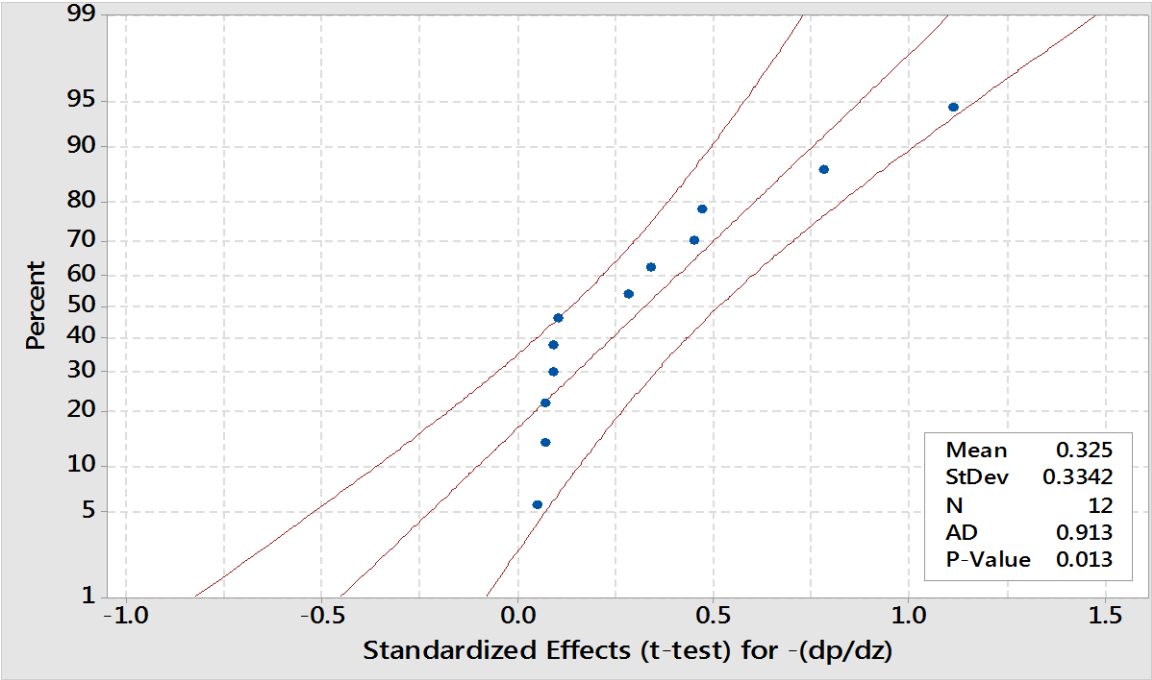

A)

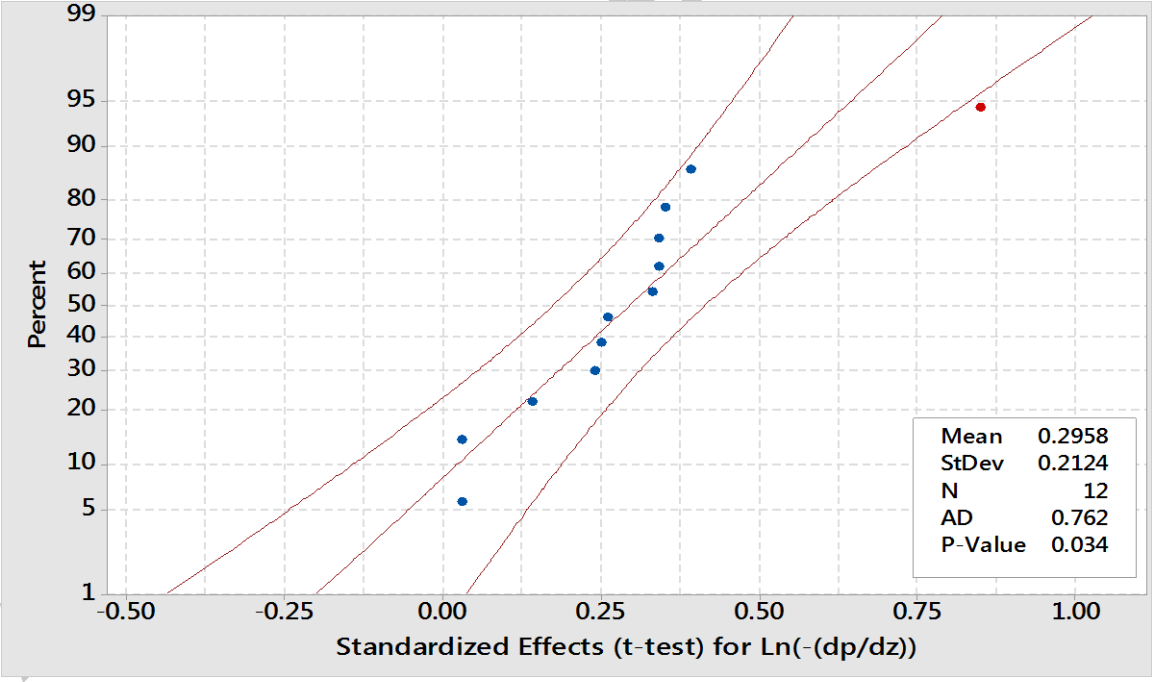

B)

Figure 6: Normal probability screening of the standardized effects with 95% confidence intervals - based on the response as in Table 2: A) –(dp/dz), B) Ln(-(dp/dz)).

From Figure 6, we notice that it becomes indifferent the choice of the dataset form (log-transformed or not) when gauging the significance of the controlling factors. All standardized effects participate in the half-normal plots by retaining their three terms (a linear and two nonlinear contributions). Their values are directly taken from the t-test estimations of Table 4. In either case, the estimated Anderson-Darling test scores (Figure 6) suggest a rejection of normality at the 0.05 significance level. Meanwhile, no particular effect seems to dramatically differentiate itself from the rest of the group when using the original dataset (Figure 6A). On the other hand, in Figure 6B, we observe that the linear part of the standardized effect of the blood behavior index poses as an outlier in the half-normal plot of the log-transformed –(dp/dz) dataset. This outcome contradicts the declared inactiveness as actually appraised by its individual significance (p-value = 0.456) from Table 4. Hence, this approach hampers the rapid factorial screening by blurring the profiler diagnostics. Consequently, a terminal decision may not be confidently delivered by simply resorting to the results of the two half-normal plots alone. The enigmatic messiness might underlie the behavior of the small datasets such the ones generated for this blood pressure-drop optimization study. Messiness might be the culprit for perplexing the discovery cycle. In turn, this aids to appreciate the robustness, agility and resilience of our proposed approach. It was demonstrated that our non-linear multi-factorial technique may be suitable to furnish a fast synchronous profiling as well as an optimal adjustment by profitably exploiting scarcely available information. The distribution-free multi-factorial slicing of the 'small-and-dense' orthogonal dataset was followed by a simple stochastic repackaging of the effects as standalone "clones". This facilitated the sturdy and rapid convergence to a robust solution. It is best exemplified by attributing high significance to the

only discovered effect which is the blood behavior index regardless of the type of treatment of the original response dataset.

It was found[21] that none of the effects essentially plays any significant role in modulating the blood pressure-drop response regardless of the dataset form. Counter-intuitively, the coefficients of determination (Table 4A) were very high in both cases. It is particularly puzzling that the predicted coefficient of determination for the original dataset is 0% while that of the log-transformed response is 99.97% (Table 4B). This is another reason to ponder that our solution differentiates from the results in reference [21]. Our predictions are valid because our solver extracts information from the screening/optimization scheme exactly on the same dataset arrangement that was planned and collected from the trials.

The best way to convince about the potential usefulness of our methodology is to demonstrate its capacity to deliver predictions much faster and with less data. To show this, we suppress the trial volume of the original experimental plan (16 runs) which were required by the $L_{16}(4^4)$ OA (Table 2) in the original report. Instead, we implement the minimum feasible orthogonal array that could accommodate all four factors such that not to omit in the investigation the potential non-linearity in the effects. This means that at least three data points per effect are necessitated. The $L_9(3^4)$ OA is the appropriate trial plan for this situation. We immediately notice that the working trial-volume requirement is downsized by a substantial amount (44%) with respect to the original $L_{16}(4^4)$ OA scheme, since now only nine runs – instead of sixteen - are needed to make the predictions. Moreover, with respect to the response surface methodology that was also adopted in the original report[21], the trial volume

reduction becomes even more pronounced (65%). To adapt the information content that has been previously generated by the $L_{16}(4^4)$ OA to the smaller $L_9(3^4)$ OA, we utilize the best fitting curve out of the two data-type versions, i.e. either from equation 19 or 20. Obviously, we select equation 20, because the transformed blood pressure drop predicts more accurately the original $L_{16}(4^4)$ OA dataset. We select two convenient endpoints for each controlling factor that relate close to the range of the original experiments and a suitable middle data-point to investigate the possibility for a non-linear behavior. The newly reconstructed dataset is now tabulated in Table 7. Repeating the analysis cycle for the $L_9(3^4)$ OA dataset, as we did for the original $L_{16}(4^4)$ OA data, we list the new outcomes in Table 8. It becomes clear again that the blood behavior index appears to be the stochastically dominant effect ($p < 0.05$). It is also confirmed that there are no error asymmetries ($p > 0.05$). Thus, the computed effect comparisons may be considered valid. We find that the blood behavior index setting of 0.5 minimizes the quantity Ln(-(dp/dx)). This agrees with the outcome of our initial analysis in the preceding section using the 16-run original dataset. We have demonstrated that our technique rapidly delivers robust results. Comparing to the original published report, our proposal reduces the amount of work in five aspects:

1) It requires a much smaller data volume.
2) It averts the double estimation effort due to: i) classical Taguchi analysis and ii) response surface methodology; it is a “single-pass” technique.
3) It is distribution-free: there is no need to search for a stochastic parametric reference law to describe the response data.

4) It is assumption-free: i) it does not require a check of normality and heteroscedasticity in Taguchi analysis and ii) it does not require residual analysis as in the response surface methodology method; it prevents the need for a subjective interpretation of the regression errors according to four customary plots: a) normal-probability plot, b) data histogram c) residuals-versus-fitted-values plot, and d) residuals-versus-observation-order plot.
5) It predicts effects equally well with or without log-transforming of the response data.

The screening results may be interpreted as that the examined range of radius of the smallest coronary-artery cross-section area may be indifferent in affecting severely the blood pressure drop. Similar conclusion may be deduced for the effect of the initial blood-flow velocity. Since the nano-particle volume fraction is not a strong influence then its appropriate setting should rest on the practicality and convenience of the method of administering the drug.

Table 7: The new nano-regulated atherosclerotic blood pressure-drop response for the $L_9(3^4)$ OA dataset.

Run #	R	V_o	N	ϕ	Ln(-(dp/dx))
1	0.001	0.2	0.5	0	5.968447
2	0.001	0.3	1	1	10.07595
3	0.001	0.4	1.5	2	13.63845
4	0.00125	0.2	1	2	8.875296
5	0.00125	0.3	1.5	0	12.9128
6	0.00125	0.4	0.5	1	5.639796
7	0.0015	0.2	1.5	1	11.93138
8	0.0015	0.3	0.5	2	4.914381
9	0.0015	0.4	1	0	8.528881

Table 8: Uncertainty and effect robust profiling for the Ln(–(dp/dz)) dataset (Table 7).

Factor	Uncertainty		Effect	
	H	p-value	H	p-value
R	0.269	0.874	2.241	0.326
V_o	3.294	0.193	0.622	0.733
n	0.605	0.739	7.2	0.0273
ϕ	3.832	0.147	0.089	0.957

With respect to the direction of the blood pressure index, it becomes clear that a setting below the normal value (n=0.78) would drive the blood pressure-drop to even lower magnitudes. This of course entails direct manipulation of the blood constituents such as cholesterol, hematocrit, fibrinogen and so forth. Parallel comparison to the accuracy of the results in reference [21] cannot be accomplished. This is because there is no estimation of uncertainty for each fitting coefficient and no estimation of the screening uncertainty at all. In lack of providing a statistical hierarchy of the effects in reference [21], predictions may become spurious in absence of the evaluations of the t-test comparisons. For example, it was found that through the response surface methodology, the coefficient of determination was reported to be 99.99%. But it performed with a discrepancy in accuracy as high as 41.37% and 13.90% in the extrapolation and interpolation prediction attempts, respectively. This disparity is not deemed reasonable and hence it motivated and justified further our work.

5. Conclusions

Managing blood pressure levels in pathological hemodynamic conditions is a critical area where chemical engineering is anticipated that could contribute with new knowledge. Synchronous rapid screening and robust optimization is a technology that might be appreciated in

applications congruent to engineering a biochemical regulation of blood pressure drop. We offered new insight about how to approach fast optimization studies that rely on Taguchi-type orthogonal sampling. Based on previously published data, we demonstrated that the optimization process may be tricky and the final outcomes to be elusive. The complex nature of blood flow measurements may be the culprit that spurs such confusion. Impeding data-messiness, non-normality, and non-linearity in small samples provide the motivation for engaging robust engineering analysis methods in new ways. We found that fitting blood data with ordinary regression techniques to lead to results with profound disadvantages that may short-circuit the knowledge discovery process. We proposed a synchronous, non-linear, distribution-free screening-and-optimization method that may be suitable to treat fast-and-small unreplicated bio-flow observations.

In the worked-out paradigm, we highlighted the consistency that the robust screening/optimization solver exhibited by converging on the same outcome regardless of log-transforming the blood pressure-gradient response or not. In both cases it was found that it is the strong influence of the blood behavior index at lower than the normal physiological limit that governs the pressure drop attenuation. This result was controlled for false discovery at a significance level of 0.05. Future works may consider screening/optimization to additional controlling factors that may include indigenous blood constituents, varying further the concentrations of iron oxide as well as trying other novel nano-carriers that may enrich the local oxygen content.

Acknowledgements: We thank the Editors and the two reviewers for providing insightful comments that improved the final version of this work.

References

1. Neofyto P. Comparison of blood rheological models for physiological flow simulation. *Biorheology*. 2004; 41: 693–714.
2. Davies PF. Hemodynamic shear stress and the endothelium in cardiovascular pathophysiology. *Nat. Clin. Practice. Cardiovasc. Med*. 2009;6:16–26.
3. Apostolidis AJ, Beris AN. Modeling of the blood rheology in steady-state shear flows. *J. Rheol*. 2014;58: 607–633.
4. Mimouni Z. The rheological behavior of human blood-comparison of two models. *Open J. Biophys.* 2016; 6: 5.
5. Adams AL, Fischer GC, Vroman L. The complexity of blood at simple interfaces. *J. Colloid Interf. Sci*. 1978; 65: 468-478.
6. Stack SW, Berger SA. The effects of high hematocrit on arterial flow—a phenomenological study of the health risk implications. *Chem. Eng. Sci*. 2009;64:4701–4706.
7. Sankar DS, Lee U. Two-fluid Herschel-Bulkley model for blood flow in catheterized arteries. *J. Mech. Sci. Technol.* 2008;22:1008.
8. Klabunde RE. Normal and abnormal blood pressure. 1st edition, RE Klabunde Publications, 2013.

9. Nadeem S, Ijaz S. Nanoparticles analysis on the blood flow through a tapered catheterized elastic artery with overlapping stenosis. *Eur. Phys. J. Plus* 2014;129:249–263.

10. Nadeem S, Ijaz S. Impulsion of nanoparticles as a drug carrier for the theoretical investigation of stenosed arteries with induced magnetic effects. *J. Magn. Magn. Mater*. 2016a;410:230–241.

11. Nadeem S, Ijaz S. Theoretical examination of nanoparticles as a drug carrier with slip effects on the wall of stenosed arteries. *Int. J. Heat Mass Trans*. 2016b; 93:1137–1149.

12. Wang Y-J, Larsson M, Huang W-T, Chiou S-H, Nicholls SJ, Chao J-I, Liu D-M. The use of polymer-based nanoparticles and nanostructured materials in treatment and diagnosis of cardiovascular diseases: recent advances and emerging designs. *Prog. Polym. Sci*. 2016;57: 153–178.

13. Hahn MA, Singh AK, Sharma P, Brown SC, Moudgil BM. Nanoparticles as contrast agents for in-vivo bioimaging: Current status and future perspectives. *Anal. Bioanal. Chem.* 2011;399:3-27.

14. Anselmo AC, Mitragotri S. A chemical engineering perspective of nanoparticle-based targeted drug delivery: A unit process approach. *AICHE J*. 2016; 62:966-974.

15. Gupta AS. Role of particle size, shape, and stiffness in design of intravascular drug delivery systems: insights from computations, experiments, and nature. *Wiley Interdiscip Rev Nanomed Nanobiotechnol* 2015; 8: 255-270.

16. Cicha I, Lyer S, Alexiou C, Garlichs CD. Nanomedicine in diagnostics and therapy of cardiovascular diseases: Beyond atherosclerotic plaque imaging. *Nanotechnol. Rev.* 2013;2:449-472.

17. Nishihara H. Human pathological basis of blood vessels and stromal tissue for nanotechnology. *Adv. Drug Delivery Rev.* 2014;74:19-27.

18. Cicha J, Garlichs CD, Alexiou C. Cardiovascular therapy through nanotechnology - How far are we still from bedside? *Eur. J. Nanomed.* 2014;6:63-87.

19. Kelley WJ, Safari H, Lopez-Cazares G, Eniola-Adefeso O. Vascular-targeted nanocarriers: design considerations and strategies for successful treatment of atherosclerosis and other vascular diseases. *Wiley Interdiscip Rev Nanomed Nanobiotechnol* 2016; 8: 909-926.

20. Ijaz, S., Nadeem, S. A biomedical solicitation examination of nanoparticles as drug agents to minimize the hemodynamics of a stenotic channel. *Eur. Phys. J. Plus 2017;*132:448–461.

21. Nematollahzadeh A, Dabaleh A, Ahadi-Jomairan N, Torabi S. Iron-oxide nano-particles effect on the blood hemodynamics in atherosclerotic coronary arteries. *Chem. Eng. Sci.* 2018; 177: 293–300.

22. Kanaris, A.G., Anastasiou, A.D., Paras, S.V. Modeling the effect of blood viscosity on hemodynamic factors in a small bifurcated artery. *Chem. Eng. Sci*. 2012; 71: 202–211.

23. Schrauwen JTC, Wentzel JJ, van der Steen AFW, Gijsen FJH. Geometry based pressure drop prediction in mildly diseased human coronary arteries. *J. Biomech*. 2014;47:1810–1815.

24. Pereira JMC, Serra e Moura JP, Ervilha AR, Pereira JCF. On the uncertainty quantification of blood flow viscosity models. *Chem. Eng. Sci*. 2013; 101:253–265.

25. Hoaglin, D.C., Mosteller, F. and Tukey, J.W. (2000), Understanding Robust and Exploratory Data Analysis, Wiley-Interscience, Hoboken, NJ.

26. Rao RS, Kumar CG, Prakasham RS, Hobbs PJ. The Taguchi methodology as a statistical tool for biotechnological applications: A critical appraisal. *Biotechnol. J.* 2008; 3:510-523.

27. Taguchi G, Chowdhury S, Taguchi S. Robust Engineering: Learn How to Boost Quality While Reducing Costs and Time to Market. New York: McGraw-Hill; 2000.

28. Taguchi G, Chowdhury S, Wu Y. Quality Engineering Handbook. Hoboken: Wiley-Interscience; 2004.

29. Briggs W. Uncertainty: The soul of modeling, probability and statistics, 1st ed. Switzerland: Springer International; 2016.

30. Floudas CA. Research challenges, opportunities and synergism in systems engineering and computational biology. AICHE J 2005:51; 1872-1884.

31. Box GEP, Hunter WG, Hunter JS. Statistics for experimenters – design, innovation, and discovery, 2nd ed. New York: Wiley; 2005.

32. Silver N. The signal and the noise: Why so many predictions fail-but some don't, 1st ed. New York: Penguin; 2015.

33. Besseris GJ. A distribution-free multi-factorial profiler for harvesting information from high-density screenings. PLoS One 2013; 8: e73275.

34. Milliken GA, Johnson DE. Analysis of Messy Data Volume I: Designed Experiments. Boca Raton: Chapman and Hall/CRC; 2004.

35. Milliken GA, Johnson DE. 1989. Analysis of Messy Data, Volume II: Nonreplicated Experiments. Boca Raton: Chapman and Hall/CRC; 1989.

36. Zeng J, Xie L, Kruger U, Gao C. Regression-based analysis of multivariate non-Gaussian datasets for diagnosing abnormal situations in chemical processes. AICHE J 2014:60; 148-159.

37. Pernot P, Cailliez F. A critical review of statistical calibration/prediction models handling data inconsistency and model inadequacy. AICHE J 2017:63; 4642-4665.

38. Steimel J, Engell S. Optimization-based support for process design under uncertainty: A case study. AICHE J 2016:62; 3404-3419.

39. Gao Y, Mi Y, Lakerveld R, An optimization-based approach for structural design of self-assembled DNA tiles. AICHE J 2017:63; 1804-1817.

40. Marcoulaki EC, Kokossis AC. Scoping and screening complex reaction networks using stochastic optimization. AICHE J 1999:45; 1977-1991.

41. Besseris GJ. A fast-and-robust profiler for improving polymerase chain reaction diagnostics. PLoS One 2014: 9; e108973.

42. Ketokivi M, Choi T. Renaissance of case research as a scientific method. J Oper Manage 2014:32; 232-240.

43. Wilcox RR. Fundamentals of Modern Statistical Methods: Substantially improving power and accuracy. London: Springer; 2010.

44. Benjamini Y, Hochberg Y. Controlling the false discovery rate: A practical and powerful approach to multiple testing. J Royal Stat Soc 1995;57:289-300.

45. World Health Organization. The top 10 causes of death. ttp://www.who.int/en/news-room/fact-sheets/detail/the-top-10-causes-of-death (Accessed: 9/21/2018).

46. Toulfatzis A, Pantazopoulos G, Besseris, G, Paipetis A. Machinability evaluation and screening of leaded and lead-free brasses using a non-linear robust multifactorial profiler. Int J Adv Manuf Technol 2016;86:3241-3254.

Highlights

- Fast and robust profiling is useful in hemodynamic monitoring and optimization
- Taguchi-type experimental designs speed up blood flow pressure drop data collection
- Translating data demands robust and agile techniques to decipher governing relationships
- Guarding against spurious effects from uncertainty asymmetry is important in small, dense and messy datasets.
- Testing published data from four examined factors, only the blood behavior index was found to be strongly significant at minimizing the blood pressure drop, at 385 Pa/m for the optimal setting of 0.5.